RSC Advances

PAPER

Cite this: *RSC Adv.*, 2016, **6**, 36248

Preparation and characterization of a covalent edge-functionalized lipoic acid–MoS_2 conjugate†

Misoon Jeong, Somin Kim and Sang-Yong Ju*

Received 12th January 2016
Accepted 5th April 2016

DOI: 10.1039/c6ra00901h

www.rsc.org/advances

Covalent functionalization of semiconducting MoS_2 is important in order to broaden the optoelectronic applications of this material. In the current study, we developed a one-step method for covalent edge functionalization of semiconducting MoS_2 with lipoic acid (LA). The process, which utilizes a simple sonochemical aqueous dispersion approach, generates a LA–MoS_2 conjugate that has a few layered nanoflake structure with a width of a few hundred nanometers and that display an intact crystalline basal plane. The MoS_2 conjugate has the tendency to stack and fold with random relative angles owing to the presence of LA edge linked groups.

Introduction

Molybdenum disulfide (MoS_2), a widely studied transition metal chalcogenide, has gained extensive interest over the last decade.[1] Aside from its concurrent applications, such as a lubricant[2] and catalyst,[3] MoS_2 has semiconductor properties. When combined with its ability to be grown and deposited over large areas,[4] MoS_2 holds high potential for use in field effect transistor and sensor applications.[5,6]

The optoelectronic property of MoS_2 is a consequence of the fact that it possesses polytype lattice structures including 1T (one layer per repeat unit, octahedral coordination), 2H (two layers per repeat unit, trigonal prismatic coordination) and 3R (three layers per repeat unit, trigonal prismatic coordination),[7,8] whose Arabic number indicates layer number per repeat. While the 1T phase exhibits metallic properties, the thermodynamically stable 2H phase[9,10] displays semiconducting properties which cause a change in the bulk indirect band gap structure to a monolayer direct band gap structure.[11,12] As a result of these features, it is possible to control the optoelectronic properties of MoS_2 by altering layer numbers,[6,11] doping,[13] changing the polytype,[9,14–16] introducing functionality[17] and strain.[18,19]

A large effort has been made to devise methods to disperse MoS_2 in various media in order to broaden its practical applications. Various solution exfoliation procedures, including those that involve the use of metal intercalation,[14–16] organic solvents,[20–22] and covalent[17,23,24] and noncovalent[25,26] functionalization. Representative of these approaches are exfoliation techniques that rely on reduction of MoS_2 by using alkali metals (*i.e.*, Li and Na).[14–16] These methods produce the metallic monolayer 1T phase of MoS_2 predominantly. Unfortunately, additional thermal annealing on a substrate[14,17] or chemical functionalization[17,24] is required to convert the monolayer 1T phase into the semiconducting 2H phase. A majority of the approaches to covalent functionalization of MoS_2 utilize initial metal-based, pre-exfoliation to generate the 1T phase followed by reactions with, for example, alkyl halides,[17] diazonium salt[24] thiols,[18] and lipoic acid (LA)[27,28] to produce the semiconducting phase. However, this chemical covalent functionalization technique produces MoS_2 with a high degree of defects on its basal plane.[24] Consequently, a facile solution-based approach for the preparation of chemically functionalized semiconducting MoS_2 with a small number of defects is needed in order to extend applications of this material.

In the study described below, X-ray diffraction (XRD), high-resolution (HR) TEM and X-ray photoelectron spectroscopy (XPS) were employed to investigate in depth the local MoS_2 structure in a conjugate with LA and structure–property relationships. For this purpose, MoS_2 was functionalized with LA using sonochemical aqueous dispersion based procedure. The results of XRD analysis showed that the LA–MoS_2 conjugate forms an one layer per repeat, trigonal prismatic 1H structure with random stacking and folding. Close inspection of HR-TEM images reveals that stacked and folded LA–MoS_2 has a twisted layer configuration and an edge covalent linkage between MoS_2 and LA, along with an intact crystalline basal plane. The material was shown by using by XPS analysis to have 10% degree of covalent edge functionalization. Finally, the combined results of atomic force microscope (AFM) and Raman studies show that the LA–MoS_2 conjugate has a nanoflake like, few-layered structure with a width of a few hundred nanometers.

Department of Chemistry, Yonsei University, 50 Yonsei-ro, Seodaemun-Gu, Seoul 03722, Korea. E-mail: syju@yonsei.ac.kr

† Electronic supplementary information (ESI) available: UV-vis-NIR extinction spectra and corresponding zeta potential table, FT-IR spectra, TGA analysis, additional TEM and AFM images. See DOI: 10.1039/c6ra00901h

Results and discussion

Lipoic acid (LA) (Fig. 1a) is an important naturally occurring organosulfur compound that is required in a number of biochemical process involved in aerobic metabolism and it used as antioxidant.[29] LA has been utilized as a ligand for coordination with quantum dot. In addition, it has been linked to the CdSe core–ZnS shell using a disulfide bond. Coordination to LA causes the stabilities of quantum dots to be enhances and it creates a site for chemical functionalization.[30] Therefore, biologically compatible LA is expected to covalently-link MoS_2, and provide anionic stable dispersion due to carboxylic acid moiety of LA, which can be further functionalized by carbodiimide chemistry. This conjugate will be useful for Bio-[23,27] and optoelectronic[24] applications. Unlike in earlier studies where a two-step approach was used to form the IT MoS_2 polytype, in the current investigation LA was used directly to covalently edge-functionalize and disperse as-supplied MoS_2 (as-MoS_2) in aqueous media. A facile sonochemical method was utilized for this purpose. As illustrated in Fig. 1a, sonication of a mixture of LA and as-MoS_2 with an average size of *ca.* 6 μm in deionized water for 3 h, followed by adjusting the pH to 6.5, and subsequent centrifugation (optional) produces a stable (up to few months) aqueous dispersion.

Zeta (ζ) potential values of the dispersion [Fig. S1 of ESI†] range from −41 to −31 mV, irrespective of centrifugation speed [3 to 100k*g*, where *g* is gravitational force (9.8 m s^{-2})] used. The negative sign of the ζ values originate from the fact that LA–MoS_2 in the dispersion contains carboxylate groups (Fig. 1a). Importantly, it is known that when its absolute ζ value is greater than 30 mV, a dispersion maintains good colloidal stability.[31] The reason for being slight decrease (from −41 to −31 mV) in ζ potential values as increasing *g* force seems to originate from stacking degree of edge-functionalized LA–MoS_2 conjugate as will be explained in later section. It is well-known that higher centrifugal force precipitates large MoS_2 bundles. Therefore, bundled LA–MoS_2 which is abundant in lower *g* force has stacked LA–MoS_2 with large number of edge-functionalized carboxylate, leading to higher ζ value whereas few-layered LA–MoS_2 obtained by higher *g* force has smaller ζ value.

The optimal dispersion protocol was obtained by changing sonication time and LA amount. Fig. S2a and b† show UV-vis-NIR extinction spectra by varying sonication time (0.5, 1, 3, and 6 h) and LA amount (0.5, 1, 5, 10, 80 mM), respectively. While increasing LA amount results in slightly increased optical density of extinction spectra, prolonged sonication time leads to proportional optical density increase of the resulting dispersion. This suggests that sonication time is more effective to achieve higher yield of LA–MoS_2 conjugate dispersion than varying LA amount. Finally, the dispersion containing the LA-functionalized MoS_2 conjugate (Fig. 1b), prepared by optimal condition (*i.e.*, 3 h sonication of a mixture of 5 mM LA, 50 mg MoS_2 in 30 mL water with pH 6.5, followed by 1 h 10k*g* centrifugation), has a dense greenish black color.

Information showing that LA-functionalized MoS_2 has randomly-stacked trigonal prismatic 1H configuration was obtained by using XRD. A thin film of LA–MoS_2 was prepared by transferring a mat obtained by filtering a dispersion through a solvent-dissolvable membrane to a glass substrate (see Experimental). The XRD pattern of the as-MoS_2 powder, utilized as a control (Fig. 2a), displays various and strong (*hkl*) peaks. Analysis of the diffractogram suggests the existence of not only interlayer ordering such as (00*l*) but also in-plane related higher ordering (*i.e.*, (113), (134), *etc.*), the intensities and positions of the peaks match those of semiconducting 2H MoS_2 (red) that has a $P6_3/mmc$ space group [provided by Joint Committee on Power Diffraction Standards (JCPDS) card no. 37-1492]. The strongest (002) peak in the pattern is positioned at 14.34° and corresponds to $d_{(002)} = 6.17$ Å of the 2H MoS_2 structure.

In contrast to that of as-MoS_2, the XRD pattern of the LA-functionalized MoS_2 is consistent with the existence of a randomly stacked 1H structure devoid of interlayer ordering, as shown in inset of Fig. 2b. XRD pattern of LA–MoS_2 (Fig. 2b) contains broadened peaks for (002), weaker higher order (00*l*) MoS_2 peaks (see ×10 spectrum), and the absence of peaks associated with various (*hkl*) diffractions except for the (00*l*) peaks. The fact that in-plane 2H MoS_2 ordering [*i.e.*, (*hkl*)], does not occur in LA–MoS_2 yet out-of-plane ordering is retained in the latter material indicates that the random stacking of layers takes place in LA–MoS_2. Folding and stacking of MoS_2 are

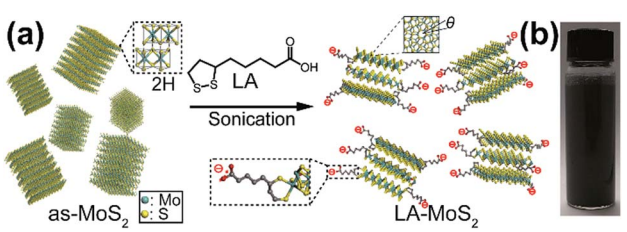

Fig. 1 (a) Schematic illustration of covalent edge functionalization of the LA–MoS_2 conjugate. θ denotes the twist angle between two MoS_2 layers. (b) Photograph of the LA–MoS_2 dispersion in water.

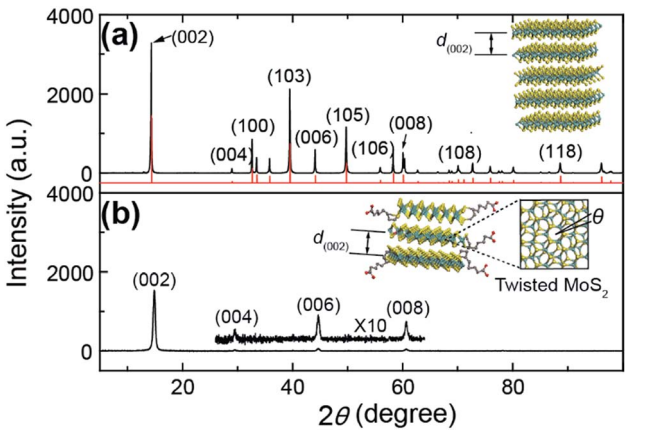

Fig. 2 XRD patterns of (a) as-MoS_2 powder and (b) LA–MoS_2 film. The peak pattern given in red in (a) is the XRD intensity spectrum of 2H MoS_2 powder obtained from JCPDS card. Insets in (a) and (b) are pictorial illustrations of the alignments of MoS_2 suggested from each XRD pattern.

spontaneous processes, which have been observed previously.[24,32] Because the surface energy (46.5 mJ m^{-2} at 298 K)[33] of the basal plane of few-layered MoS_2 is markedly different from that of water (72 mJ m^{-2}), edge-functionalized exfoliated LA–MoS_2 seems to have a tendency to stack and fold with random configurations in an aqueous environment. A similar trend exists in edge-functionalized graphene,[34,35] whose XRD pattern contains a (001) diffraction peak position that is the same as that of graphite, a broadened (00*l*) diffraction peak, while various (*hkl*) diffraction peaks are absent. Based on the XRD observations, it appears that chemical modification of MoS_2 with LA leads to formation of an edge-functionalized crystalline structure (right inset of Fig. 2b).

Moreover, although the position of the (002) peak in the XRD pattern of LA–MoS_2 is similar to that of as-MoS_2, its full-width at half maximum (FWHM: 0.48°) is greater than that (0.16°) of the (002) peak of 2H as-MoS_2. Analysis using Debye–Scherrer's equation,[36] which shows that the crystallite domain size is inversely proportional to the FWHM, broadening of (002) peak in the XRD pattern of LA–MoS_2 suggests that it exists in smaller size crystals compared to as-MoS_2. In addition, the similarity between its (002) peak position and that of as-MoS_2 indicates that negligible LA intercalation between basal plane of MoS_2 layers exists in LA–MoS_2. This observation contrasts starkly with those made in studies of basal-plane metal-intercalated MoS_2,[37] whose XRD (002) peak position is shifted to a smaller angle.

In Fig. 3 are displayed TEM images of the LA–MoS_2 conjugate. Analysis of the images shows the stacking and folding configurations of this material along with the edge location of the functionality. The low magnification TEM image (Fig. 3a) contains several few-layered MoS_2 flakes with lateral lengths of several hundred nanometres. LA–MoS_2 nanoflakes exhibit dominant stacking and folding features. In addition, straight lines (red arrows) seen in the images originate from folded MoS_2 edges and the irregular boundary stems from bare edges. The basal plane of a LA–MoS_2 flake (Fig. 3b) is comprised of a hole-free, well-arranged hexagonal MoS_2 sheet along with minor organic residues on the surface. The fact that that crystalline LA–MoS_2 is free of basal defects contrasts with the properties of materials made from lithiated MoS_2 by using other basal plane functionalization methods.[24,32] Materials made using these approaches have basal planes that contain holes and cracks.[24] This finding suggests that the basal plane of MoS_2 in flakes of the LA–MoS_2 conjugate remains unreacted during the functionalization process. This result is consistent with the observation that position of the (002) peak in the XRD pattern of LA–MoS_2 is similar to that of as-MoS_2. The corresponding fast Fourier-transform (FFT) image contains two sets of intensity-different six-fold symmetry patterns. The six-fold symmetry originates from the (100) diffraction that has a relative rotation angle of *ca.* 15.4°. Thus, the MoS_2 layers are randomly stacked during functionalization with LA (see additional TEM images in Fig. S2b and d of ESI†). The combined results demonstrate that LA edge functionalization is benign method that preserve the in-plain crystallinity of MoS_2.

Consistent with the observations summarized above is the fact that the folded edges (Fig. 3c) of the LA–MoS_2 conjugate are relatively clean and contain fewer functional groups. Interestingly, closer inspection of the folded edges reveals that the edge terrace of the MoS_2 layers (red arrows) and folded vertex (yellow arrows) possess a large number of physisorped LA, suggesting that functionalization by LA occurs at dangling bond sites of MoS_2 edge. The bare edge (Fig. 3d) of the conjugate also contains irregularly-shaped physisorped LA at the end of the crystalline MoS_2 boundary, along with aforementioned twisted few-layered MoS_2 with a rotation angle of 18.6° (inset). Moreover, localized folding features exist on the MoS_2 sheet (Fig. 3e) with *ca.* 6.5 Å spacing, which closely matches the XRD

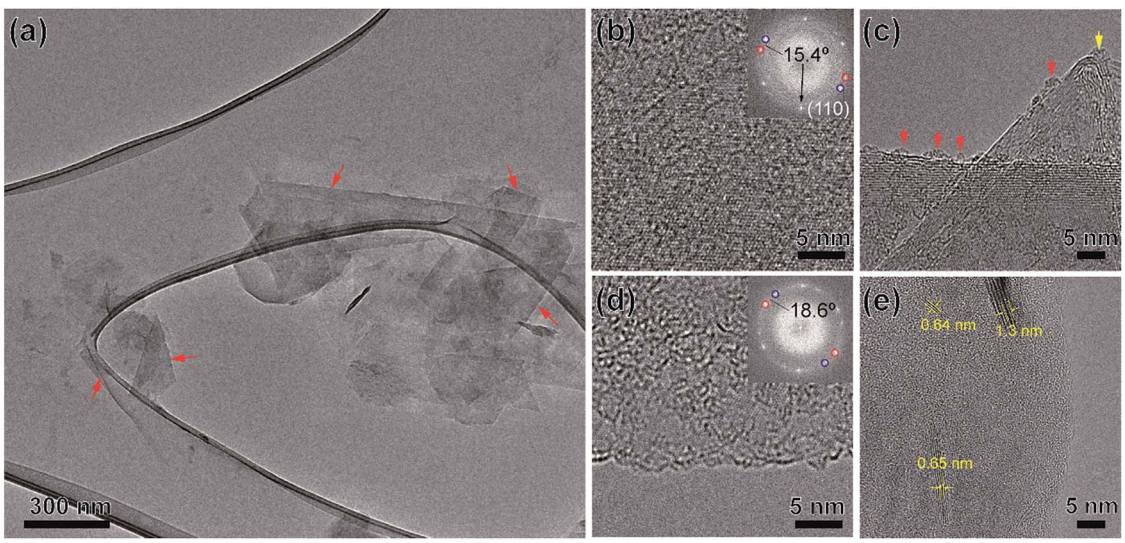

Fig. 3 TEM images showing the morphologies of LA–MoS_2 flakes. (a) Low magnification TEM image of several LA–MoS_2 flakes. HR-TEM images of (b) basal plane, and (c) folded edges. Inset: Fourier transform pattern. (d) Edges of twisted few-layered LA–MoS_2, and (e) localized folded structures (yellow marker) on the MoS_2 plane.

determined interlayer distance of 6.2 Å. The variation in the layer spacing between folds is likely a consequence of differently-spaced twisted MoS_2 layers,[38] along with the acuteness of the folded structure. Overall, direct evidence has come from the TEM analysis to show that LA–MoS_2 nanoflakes have a randomly-rotating stacked and folded layer configuration with various types of edge LA-functionalization including bare, terrace, and folded apex.

The results of XPS studies provide information about the nature of the covalent edge functionalization in the LA–MoS_2 conjugate. In Fig. 4a and b are displayed the Mo3d, S2s, and S2p regions of the XPS acquired using as-MoS_2 and LA–MoS_2 samples. Deconvolution using a voigt fit shows that the Mo spectrum of as-MoS_2 is comprised of peaks at 232.7 and 229.5 eV (red lines), which agree well with the expected 2H MoS_2 doublet peak arising from $Mo^{4+}3d_{3/2}$ and $3d_{5/2}$ as a consequence of spin–orbit coupling.[39] The 0.78 ratio of the areas in the d doublet of the individual peaks is slightly larger than the predicted value of 0.66.[40] Similar to that observed for Mo, the S2p doublet in the spectrum of as-MoS_2 is comprised of two major peaks at 163.6 and 162.4 eV, which correspond to $2p_{1/2}$ and $2p_{3/2}$, respectively, associated with the 2H phase. It is noteworthy that oxidation-related peaks of Mo (*ca.* 236 eV) and S (*ca.* 168 eV) are negligible.

The Mo3d spectrum of LA-functionalized MoS_2 (Fig. 4b) contains peaks at 232.7 and 229.6 eV, which are nearly identical to those of the as-MoS_2 2H peaks. This finding indicates that covalent functionalization of MoS_2 by LA does not alter innate 2H polytypes. The position of the S2s peak is increased by *ca.* 0.9 eV and its intensity is enhanced in comparison to that (226.7 eV) of as-MoS_2. The reason for the intensity increase is associated with the extra sulfur contained within unreacted LA.

The S2p spectrum reveals three sulfur species in LA–MoS_2 conjugate. The deconvoluted S2p spectrum is comprised of three sets of doublets (Fig. 4d, purple, green, and red with 1.0, 1.4, and 1.1 eV doublet peak separations, respectively). The lower binding energy doublet (red) is comprised of peaks at 163.4 and 162.4 eV that are nearly identical to the position of the peaks in the 2H MoS_2 doublet. Purple doublet (164.7 and 163.6 eV) is upshifted by 1.2 eV as compared to that of the 2H MoS_2 doublet and originates from unbound, excess LA, based on its position.[41]

Green doublet upshifted by 0.7 eV as compared to that of 2H MoS_2 doublet originates from covalently conjugated sulfur between LA and MoS_2. Green doublet positions (162.7 and 164.1 eV) are situated between doublets originating from excess LA (purple doublet) and 2H MoS_2. This doublet are alike that of alkyl-functionalized S2p of MoS_2 (*i.e.*, 162.9 and 164.0 eV),[17,24,40] indicating successful edge covalent functionalization of LA on MoS_2 by forming Mo–S-alkyl covalent bridge. A comparison of the area of the functionalized sulfur doublet peak (green) with those associated with the 2H structure (red) indicates that *ca.* 10% of total sulfur content stems from covalent functionalization. In addition, the large oxidation peak of S2p (inset of Fig. 4b) observed at 168.7 eV originates from sulfate species formed from LA[42] upon exposure of the sample to air and water.[43] The presence of sulfate derivatives of LA–MoS_2 could be responsible for additional anionic dispersion stability in the water.

Further characterizations of covalent LA–MoS_2 conjugate were performed with Fourier Transform Infrared spectroscopy (FT-IR) (see Experimental for sample preparation). Fig. S4a to c† shows IR spectra of as-MoS_2, LA salt, and LA–MoS_2 conjugate. IR spectrum from MoS_2 shows flat baseline except 464 cm^{-1}, corresponding to Mo–S stretch vibration.[44] On the other hands, LA salt and LA–MoS_2 share similar vibrational features originating from LA. LA salt sample shows stretch vibration of aliphatic C–H at 2926 and 2853 cm^{-1}, and LA–MoS_2 shows those features at 2924 and 2854 cm^{-1}.[23] In addition, LA salt shows a broad carboxylate stretch band at 1564 cm^{-1}, and LA–MoS_2 displays the same band at 1556 and 1624 cm^{-1}.[45] These results indicate that LA are successfully functionalized onto MoS_2. Moreover, unlike the case of LA salt, LA–MoS_2 shows strong protonated and salt form of sulfate peak at 1261, 1089 and 1049 cm^{-1}, in line with previous sulfate peak on LA-quantum dot conjugate,[42] confirming the sulfate moiety formation discussed in the XPS result. The magnified IR spectra from 400 to 600 cm^{-1}, due to low response of S–S bond shows that LA salt displays multiple peaks (486 and 449 cm^{-1}), corresponding to S–S stretch vibration of LA.[45] The reason for being two peaks seems to originate from isomer of lipoic acid we used. In the meanwhile LA–MoS_2 displays only 470 cm^{-1}, originating from Mo–S stretch vibration, without any bands from S–S stretch. This indirectly supports that S–S bond disappears by conjugating LA with MoS_2. Moreover, the LA functionalization degree of the resulting LA–MoS_2 conjugate was confirmed by using TGA analysis. Fig. S5† shows weight (wt) loss trace of LA–MoS_2, along with those of LA salt and as-MoS_2 for comparison, with 5 °C ramping rate under nitrogen atmosphere. First, LA salt shows three major wt losses at 262, 437, and 722 °C, whose remaining wt% are 91.6, 58.7, and 31.8, respectively. For comparison, as-MoS_2

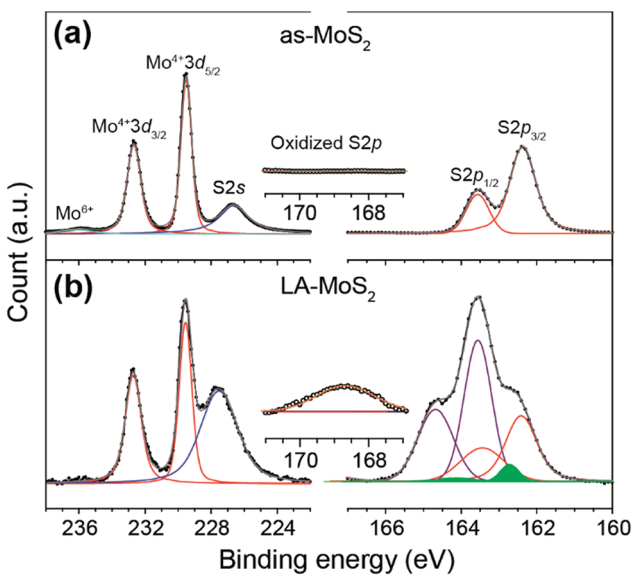

Fig. 4 XPS of (a) as-MoS_2 and (b) LA–MoS_2. Black dots: original data, grey curves: integrated value of voigt curve fitting.

starts to show gradual weight loss at 475 °C, which is similar to that of MoS_2 in the literature.[32,46] On the other hand, LA–MoS_2 shows 98.9% remaining weight at 262 °C which corresponds to first wt loss of LA salt. Based on this, we estimate that sulfur of MoS_2 is functionalized with LA by 8.7%, which is in good agreement with 10% functionalization determined by XPS results.

AFM analysis confirms that the formed LA–MoS_2 flakes mainly consist of a few layers. For obtaining accurate measurements, the LA–MoS_2 sample was dropcast on piranha-cleaned 285 nm thick SiO_2/Si substrate. The resulting sample was washed with copious amounts of water and dried (see Experimental for detail). Inspection of the height topography (Fig. 5a) show that the LA–MoS_2 flakes are irregularly shaped (see Fig. S3† for additional AFM image) in a manner that is similar to dispersed MoS_2 flakes generated by using sonochemistry.[26] In some cases, the LA–MoS_2 nanoflakes form large aggregates (Fig. S3b†). Finally, the flakes (Fig. 5b) have an average height of 2.0 nm, which corresponds to that of trilayered MoS_2.[6,47]

The Raman spectrum (Fig. 5c) of LA–MoS_2, excited by 532 nm, contains a band at 383.7 cm^{-1}, corresponding to an in-plane E^1_{2g} mode, and at 405.6 cm^{-1} for an out-of-plane A_{1g} mode.[42,43] It is well-known that as the layer numbers of MoS_2 increase the respective E^1_{2g} and A_{1g} peaks shift to lower and higher frequencies. Moreover, the interpeak separation can be used to determine the numbers layer that exist in the nanoflake.[47,48] By using this relationship, the observed peak separation of *ca.* 22 cm^{-1} corresponds to three layers[6,47] value that compares well with that determined from AFM measurements. Height profile analysis of 50 different flakes shows that height (Fig. 5d) is 1.8 nm, the full-width at half maximum is 0.6 nm, and the average lateral length (Fig. 5e) is *ca.* 240 nm. The latter value is much smaller than that of as-MoS_2 (*ca.* 6 μm).

Following an evaluation of its solid properties, LA–MoS_2 dispersion was subjected to optical characterization. In Fig. 6a is given the UV-vis-NIR extinction spectra of aqueous the LA–MoS_2 dispersion following centrifugation at 10 000*g*. Bands in the extinction spectrum of the dispersion are centred at 387, 431, 609, and 667 nm that lie on top of broad extinction band. The four peaks correspond to D, C, B, and A excitons of MoS_2 (ref. 12, 49 and 50) in that order. Those positions are in good agreement with those (*ca.* 610 and 660 nm) observed in chemically exfoliated few-layered MoS_2.[39,40] This observation supports the conclusion that the LA–MoS_2 conjugate has a few-layered structure. As seen by inspection of the energy dispersion diagram displayed in Fig. 6b, while the D and C excitons originate from indirect transitions at a near zone center Γ and Λ in the Brillouin zone,[49] the A and B excitons[11,12] stem from direct transitions at zone boundary K due to spin–orbit coupling separated by *ca.* 160 meV. Under 635 nm laser irradiation, the sample of LA–MoS_2 displays strong scattering (data not shown). The fact that extinction spectrum extends beyond the band edge (660 nm) suggests that this materials is comprised of particles that have a sufficiently large size to scatter incident light. However, the LA–MoS_2 sample does not photoluminescence at 660 and 840 nm, which would originate from direct and indirect transitions.[11] The absence of emission is presumably a result of the stacking and folding nature of the conjugate. In any event, analysis of the extinction spectrum provides information that is in line with the results of the TEM and AFM experiment and suggests that the LA–MoS_2 conjugate is composed of particles whose sizes are comparable to the excitation light of a few hundred nm.

The remaining question to be answered is how MoS_2 sheet is only edge-functionalized with LA. Previous work has suggested unstable Mo-terminated edges with higher sulfur affinities.[23,51] Highly energetic ultrasonication renders various vacancies, defects, and tears in MoS_2. For instance, when MoS_2 sheet is torn upon sonication (Fig. 7a), it produces both sulfur

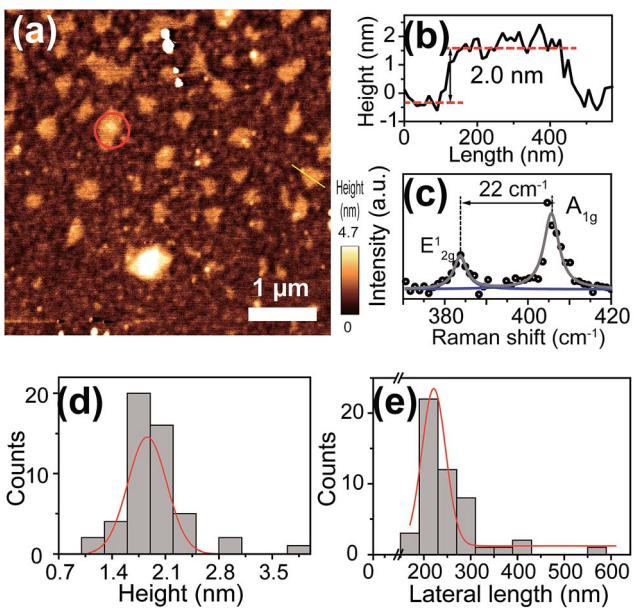

Fig. 5 (a) AFM height topography of LA–MoS_2 flakes on a 285 nm thick SiO_2/Si substrate. (b) Height profile along yellow line in (a). (c) Raman spectrum of circled part in (a) excited by using a 532 nm laser. (d) Height and (e) length histograms of 50 different LA–MoS_2 flakes.

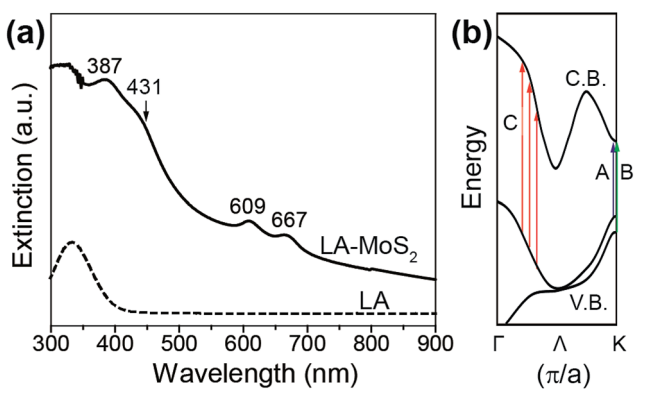

Fig. 6 (a) UV-vis-NIR extinction spectra of LA–MoS_2 (solid) and LA (dash). (b) The corresponding energy dispersion in the Brilloiun zone. C.B. and V.B. denote conduction and valence bands, respectively.

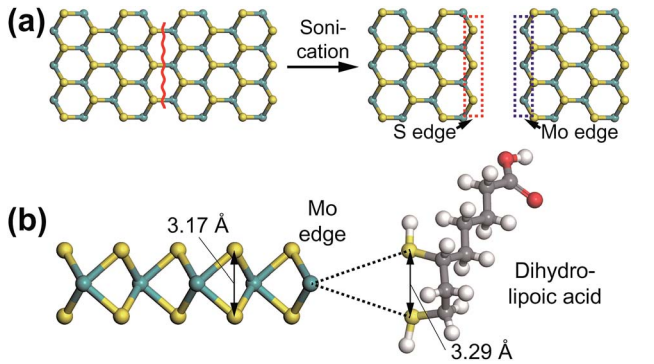

Fig. 7 Suggested mechanism for edge functionalization of LA with Mo edges of MoS_2. (a) Sonication-assisted MoS_2 tearing, producing S- and Mo-terminated edge. (b) Preferential Mo edge functionalization with dihydrolipoic acid due to favourable geometry.

terminated and Mo terminated edges. Mo terminated edges need energetically favourable "dimeric sulfur" (*i.e.*, two sulfurs connected to same Mo), according to theoretical calculation.[51] Energy gain for Mo edge to form dimeric sulfur is *ca.* 269 kJ mol^{-1},[51] and is enough to form two Mo–S bonds of LA (Fig. 7b). Moreover, the distance between the nearest sulfurs linked to a Mo in 2H MoS_2 sheet is *ca.* 3.17 Å. This is similar distance (3.29 Å) between sulfur moieties of dihydrolipoic acid whose configuration was obtained by energy-minimization at the Hartree Fock (HF)/STO-3G level of theory (see Experimental). This can facilitate LA functionalization to MoS_2 edges without additional energetic cost. Moreover, the aforementioned random stacking of LA–MoS_2 sheet is also expected to assist edge functionalization by protecting basal plane. This is in good agreement with favourable edge functionalization over basal plane observed in previous literature.[52–55]

Conclusions

In the investigation described above, we have devised a simple, one-step, sonication method to produce a lipoic acid edge-functionalized, semiconducting MoS_2 dispersion. In this process, LA covalently bonds to the edges of MoS_2 to produce a LA–MoS_2 conjugate that has stacked and folded layers aligned with a random relative rotation angle owing to the absence of basal plane chemical functional groups. The dispersion behaves as a stable anionic colloid because of the presence of the carboxylate moiety of the LA component. That LA–MoS_2 possesses a relative rotation angle is evidenced by the interesting (00*l*) XRD pattern, along with twisted six-fold symmetry pattern observed by using HR-TEM. Especially, interesting is the fact that covalent linked LA groups are localized along various edges of the conjugate (*i.e.*, bare, terrace, and vertex edges). The LA–MoS_2 conjugate displays typical few-layered characteristics such as the height of the flakes being *ca.* 2.0 nm and a Raman interpeak separation of 22 cm^{-1}. This study provides a protocol for fabrication of edge-functionalized MoS_2 with high degree of crystallinity. This finding should serve as a method for forming solution-processable chemically functionalized MoS_2 which has potentially important uses in optoelectronic and biochemical applications.

Experimental

1. Materials and methods

MoS_2 powder [Cat. #: 69860, size: *ca.* 6 μm (max. size: 40 μm)] was obtained from Sigma Aldrich. Isomeric mixture of LA (DL-α-LA, 98%) was purchased from Wako Pure Chemicals. Deionized water having resistance greater than 18.2 MΩ was used to disperse MoS_2. ζ potentials were acquired using a Zen3600 zetasizer (Malvern instruments). The sample was introduced into a zeta dip cell (ZEN1002) with thermal controller and stabilized at 25 °C in order to reach thermal equilibrium. The potential values were determined by averaging the results of several measurements. Raman measurements were made using a custom-made setup with 532 nm laser and 1800 lines per mm grating, according to previous work.[56] Prior to Raman and AFM measurements, a 150 μL sample was dropcasted on a 285 nm thick SiO_2/Si substrate (P^{++}-doped, Shinetsu) and then subjected to drying by using a nitrogen stream. A 50 μW laser was used to prevent unwanted sample damage. UV-vis-NIR extinction spectra were acquired using a JASCO V-770 with a cuvette having 1 cm path length. For the FT-IR and TGA measurements, the filtered LA–MoS_2 sample on a filter paper was washed with copious amounts of water and ethanol several times, in order to remove unreacted LA. LA was neutralized to form LA sodium salt by reacting with sodium hydroxide, for comparison purpose of LA–MoS_2 salt form. Samples are ground with completely dried KBr power to produce a pellet for IR measurements. FT-IR spectra were acquired with Vertex 70 (Bruker) and were obtained by 32 times accumulation. TGA measurements were conducted by TGA-50 (Shimadzu). Temperature of the samples in an aluminium fans was raised from rt to 900 °C with a ramping rate of 5 °C under nitrogen atmosphere. Energy minimization of dihydrolipoic acid was conducted in vacuum by using Gaussian 09W[57] with HF/STO-3G basis set.

2. Preparation of LA–MoS_2 conjugate

Optimal method is following. A 32 mg (0.15 mmol) sample of LA was added to 30 mL deionized water and the pH of the resulting solution was adjusted to 6.5. After LA was completely dissolved, 50 mg of MoS_2 was added. The resulting mixture was tip-sonicated (probe tip diameter: 13 mm, VCX 750, Sonics & Materials) for 3 h at 300 W. The upper 80% supernatant was collected after 10k*g* centrifugation using a fixed angle rotor (Hanil supra 22k). For centrifugal force dependent measurements, samples were collected after various centrifugal forces (3, 10, 15, 30, 50, and 100k*g*) using an optional swing-bucket rotor (SW41 Ti, Beckman Coulter).

3. LA–MoS_2 film preparation

Film preparation followed a procedure developed in our earlier work.[58] A 10 mL aliquot of the LA–MoS_2 conjugate dispersion was subjected to 10k*g* centrifugation and filtered through a mixed cellulose ester membrane (pore size: 0.2 μm, lot. #:

00728200, Advantec). Washing the precipitate with copious amounts of water was utilized to remove excess LA. Before the LA–MoS_2 film on the membrane was completely dried, the sample side on the membrane was firmly pressed onto a piranha-cleaned slideglass, and then placed into acetone-vapor reflux chamber overnight so that the membrane slowly dissolved away. The resulting films were used for XRD measurements.

XRD measurements: X-ray diffractograms of the samples were obtained *via* Rigaku Ultima IV using Cu K_α radiation (λ = 1.541 Å) and scan speed of 2° min^{-1}. The sample on a slideglass was placed onto the XRD mount. The resulting spectra were compared with standards in JCPDS PDF No. 37-1492.

4. TEM measurements

HR-TEM measurements were conducted using either JEOL JEM-ARM 200F or JEOL 2100, with 200 kV acceleration voltage. Copper TEM grids covered with an ultra-thin carbon support film on a lacey carbon support [LC200-Cu (Lot#: 110727), 200 mesh, Ted Pella] were used. A 20 μL LA–MoS_2 sample was dropcast on the TEM grid. After 3 min of incubation, and excess dispersion was removed by wicking off with Kimwipers and water washing.

5. XPS measurements

XPS data were acquired with K-alpha (Thermo Scientific, U.K.). A monochromatic X-ray source (Al K_α line: 1486.6 eV), whose beam size is 400 μm, was used with power of 12 kV and 3 mA. Survey scans were acquired with 100 eV pass energy at resolution of 1 eV. Detailed scans were obtained at 20 eV pass energy with a resolution of 0.05 eV. The acquired spectra were baseline-subtracted using Shirley profile. C1s carbon peak (284.8 eV) of adventitious carbon and LA were used as internal references for as-MoS_2 and LA–MoS_2, respectively.

6. AFM measurements

AFM measurements were conducted using a commercial AFM (Nanowizard I, JPK instrument) installed onto an inverted microscope (Zeiss). Al-coated silicon AFM cantilevers (spring constant: 13–77 N m^{-1}, frequency range: 200–400 kHz, App-Nano) were used to obtain tapping mode imaging, whose pixel size are 512 × 512. Polynomial flattening routine was applied to height topography.

Acknowledgements

The authors thank YJ Jeong for initial help for sample preparation and E. Koo for energy minimization of dihydrolipoic acid. This research was supported financially by the Basic Science Research Program through the National Research Foundation of Korea (NRF) funded by the Ministry of Education, Science and Technology (2014R1A1A2055572), and in part by the Yonsei University Future-Leading Research Initiative of 2014.

Notes and references

1 K. S. Novoselov, D. Jiang, F. Schedin, T. J. Booth, V. V. Khotkevich, S. V. Morozov and A. K. Geim, *Proc. Natl Acad. Sci. USA*, 2005, **102**, 10451–10453.
2 W. O. Winer, *Wear*, 1967, **10**, 422–452.
3 D. Voiry, M. Salehi, R. Silva, T. Fujita, M. Chen, T. Asefa, V. B. Shenoy, G. Eda and M. Chhowalla, *Nano Lett.*, 2013, **13**, 6222–6227.
4 K.-K. Liu, W. Zhang, Y.-H. Lee, Y.-C. Lin, M.-T. Chang, C.-Y. Su, *et al.*, *Nano Lett.*, 2012, **12**, 1538–1544.
5 B. Radisavljevic, A. Radenovic, J. Brivio, V. Giacometti and A. Kis, *Nat. Nanotechnol.*, 2011, **6**, 147–150.
6 H. S. Lee, S.-W. Min, Y.-G. Chang, M. K. Park, T. Nam, H. Kim, J. H. Kim, S. Ryu and S. Im, *Nano Lett.*, 2012, **12**, 3695–3700.
7 D. Yi, W. Yanli, J. Jun, S. Lin, S. Siqi and T. Weihua, *Physica B*, 2011, **406**, 2254–2260.
8 Q. H. Wang, K. Kalantar-Zadeh, A. Kis, J. N. Coleman and M. S. Strano, *Nat. Nanotechnol.*, 2012, **7**, 699–712.
9 F. Wypych and R. Schollhorn, *J. Chem. Soc. Chem. Commun.*, 1992, 1386–1388.
10 F. Wypych, K. Sollmann and R. Schöllhorn, *Mater. Res. Bull.*, 1992, **27**, 545–553.
11 A. Splendiani, L. Sun, Y. Zhang, T. Li, J. Kim, C.-Y. Chim, G. Galli and F. Wang, *Nano Lett.*, 2010, **10**, 1271–1275.
12 K. F. Mak, C. Lee, J. Hone, J. Shan and T. F. Heinz, *Phys. Rev. Lett.*, 2010, **105**, 136805.
13 S. Mouri, Y. Miyauchi and K. Matsuda, *Nano Lett.*, 2013, **13**, 5944–5948.
14 K. E. Dungey, M. D. Curtis and J. E. Penner-Hahn, *Chem. Mat.*, 1998, **10**, 2152–2161.
15 Z. Zeng, T. Sun, J. Zhu, X. Huang, Z. Yin, G. Lu, *et al.*, *Angew. Chem., Int. Ed.*, 2012, **51**, 9052–9056.
16 H. S. S. Ramakrishna Matte, A. Gomathi, A. K. Manna, D. J. Late, R. Datta, S. K. Pati and C. N. R. Rao, *Angew. Chem., Int. Ed.*, 2010, **49**, 4059–4062.
17 D. Voiry, A. Goswami, R. Kappera, E. SilvaCecilia de Carvalho Castro, D. Kaplan, T. Fujita, M. Chen, T. Asefa and M. Chhowalla, *Nat. Chem.*, 2015, **7**, 45–49.
18 H. J. Conley, B. Wang, J. I. Ziegler, R. F. Haglund, S. T. Pantelides and K. I. Bolotin, *Nano Lett.*, 2013, **13**, 3626–3630.
19 A. Castellanos-Gomez, R. Roldán, E. Cappelluti, M. Buscema, F. Guinea, H. S. J. van der Zant and G. A. Steele, *Nano Lett.*, 2013, **13**, 5361–5366.
20 J. N. Coleman, M. Lotya, A. O'Neill, S. D. Bergin, P. J. King, U. Khan, *et al.*, *Science*, 2011, **331**, 568–571.
21 V. Nicolosi, M. Chhowalla, M. G. Kanatzidis, M. S. Strano and J. N. Coleman, *Science*, 2013, **340**, 1226419.
22 Z. Tang, Q. Wei and B. Guo, *Chem. Commun.*, 2014, **50**, 3934–3937.
23 S. S. Chou, M. De, J. Kim, S. Byun, C. Dykstra, J. Yu, J. Huang and V. P. Dravid, *J. Am. Chem. Soc.*, 2013, **135**, 4584–4587.

24 K. C. Knirsch, N. C. Berner, H. C. Nerl, C. S. Cucinotta, Z. Gholamvand, N. McEvoy, *et al.*, *ACS Nano*, 2015, **9**, 6018–6030.

25 K. Zhou, J. Liu, P. Wen, Y. Hu and Z. Gui, *Appl. Surf. Sci.*, 2014, **316**, 237–244.

26 J. Kang, J.-W. T. Seo, D. Alducin, A. Ponce, M. J. Yacaman and M. C. Hersam, *Nat. Commun.*, 2014, **5**, 5478.

27 T. Liu, C. Wang, W. Cui, H. Gong, C. Liang, X. Shi, Z. Li, B. Sun and Z. Liu, *Nanoscale*, 2014, **6**, 11219–11225.

28 C. Backes, N. C. Berner, X. Chen, P. Lafargue, P. LaPlace, M. Freeley, G. S. Duesberg, J. N. Coleman and A. R. McDonald, *Angew. Chem., Int. Ed.*, 2015, **54**, 2638–2642.

29 L. Packer, E. H. Witt and H. J. Tritschler, *Free Radic. Biol. Med.*, 1995, **19**, 227–250.

30 H. Mattoussi, J. M. Mauro, E. R. Goldman, G. P. Anderson, V. C. Sundar, F. V. Mikulec and M. G. Bawendi, *J. Am. Chem. Soc.*, 2000, **122**, 12142–12150.

31 D. H. Everett, *Basic pinciples of Colloid Science*, Roayl Society of Chemistry, London, 1988.

32 L. Zhou, B. He, Y. Yang and Y. He, *RSC Adv.*, 2014, **4**, 32570–32578.

33 A. P. S. Gaur, S. Sahoo, M. Ahmadi, S. P. Dash, M. J. F. Guinel and R. S. Katiyar, *Nano Lett.*, 2014, **14**, 4314–4321.

34 I.-Y. Jeon, D. Yu, S.-Y. Bae, H.-J. Choi, D. W. Chang, L. Dai and J.-B. Baek, *Chem. Mat.*, 2011, **23**, 3987–3992.

35 I.-Y. Jeon, H.-J. Choi, S.-M. Jung, J.-M. Seo, M.-J. Kim, L. Dai and J.-B. Baek, *J. Am. Chem. Soc.*, 2013, **135**, 1386–1393.

36 Y. Waseda, M. Eiichiro and S. Kozo, *X-Ray Diffraction Crystallography*, Springer Berlin Heideberg, Berlin, 2011.

37 J. Zheng, H. Zhang, S. Dong, Y. Liu, C. Tai Nai, H. Suk Shin, H. Young Jeong, B. Liu and K. Ping Loh, *Nat. Commun.*, 2014, **5**, 2995.

38 J. He, K. Hummer and C. Franchini, *Phys. Rev. B*, 2014, **89**, 075409.

39 G. Eda, H. Yamaguchi, D. Voiry, T. Fujita, M. Chen and M. Chhowalla, *Nano Lett.*, 2011, **11**, 5111–5116.

40 C. Backes, R. J. Smith, N. McEvoy, N. C. Berner, D. McCloskey, H. C. Nerl, *et al.*, *Nat. Commun.*, 2014, **5**, 4576.

41 D. G. Castner, K. Hinds and D. W. Grainger, *Langmuir*, 1996, **12**, 5083–5086.

42 J. Jiang, C. V. Conroy, M. M. Kvetny, G. J. Lake, J. W. Padelford, T. Ahuja and G. Wang, *J. Phys. Chem. C*, 2014, **118**, 20680–20687.

43 F. E. Stary, S. L. Jindal and R. W. Murray, *J. Org. Chem.*, 1975, **40**, 58–62.

44 J. Li, W. Tang, H. Yang, Z. Dong, J. Huang, S. Li, J. Wang, J. Jin and J. Ma, *RSC Adv.*, 2014, **4**, 1988–1995.

45 A. G. Young, D. P. Green and A. J. McQuillan, *Langmuir*, 2007, **23**, 12923–12931.

46 X. Wang, E. N. Kalali and D.-Y. Wang, *J. Mater. Chem. A*, 2015, **3**, 24112–24120.

47 C. Lee, H. Yan, L. E. Brus, T. F. Heinz, J. Hone and S. Ryu, *ACS Nano*, 2010, **4**, 2695–2700.

48 H. Li, Q. Zhang, C. C. R. Yap, B. K. Tay, T. H. T. Edwin, A. Olivier and D. Baillargeat, *Adv. Funct. Mater.*, 2012, **22**, 1385–1390.

49 D. Kozawa, R. Kumar, A. Carvalho, K. Kumar Amara, W. Zhao, S. Wang, *et al.*, *Nat. Commun.*, 2014, **5**, 4543.

50 A. Chernikov, T. C. Berkelbach, H. M. Hill, A. Rigosi, Y. Li, O. B. Aslan, D. R. Reichman, M. S. Hybertsen and T. F. Heinz, *Phys. Rev. Lett.*, 2014, **113**, 076802.

51 L. S. Byskov, B. Hammer, J. K. Nørskov, B. S. Clausen and H. Topsøe, *Catal. Lett.*, 1997, **47**, 177–182.

52 B. Hinnemann, P. G. Moses, J. Bonde, K. P. Jørgensen, J. H. Nielsen, S. Horch, I. Chorkendorff and J. K. Nørskov, *J. Am. Chem. Soc.*, 2005, **127**, 5308–5309.

53 T. F. Jaramillo, K. P. Jørgensen, J. Bonde, J. H. Nielsen, S. Horch and I. Chorkendorff, *Science*, 2007, **317**, 100–102.

54 Y. Li, H. Wang, L. Xie, Y. Liang, G. Hong and H. Dai, *J. Am. Chem. Soc.*, 2011, **133**, 7296–7299.

55 K. Chang, Z. Mei, T. Wang, Q. Kang, S. Ouyang and J. Ye, *ACS Nano*, 2014, **8**, 7078–7087.

56 E. Koo and S.-Y. Ju, *Carbon*, 2015, **86**, 318–324.

57 M. J. Frisch, G. W. Trucks, H. B. Schlegel, G. E. Scuseria, M. A. Robb and J. R. Cheeseman, *et al.*, Gaussian, Inc, Wallingford CT, 09W edn, 2009.

58 W. Yoon, Y. Lee, H. Jang, M. Jang, J. S. Kim, H. S. Lee, *et al.*, *Carbon*, 2015, **81**, 629–638.

Electronic Supplementary Information for

Preparation and Characterization of a Covalent Edge-Functionalized Lipoic Acid-MoS_2 Conjugate

*Misoon Jeong, Somin Kim, and Sang-Yong Ju**

Department of Chemistry, Yonsei University, 50 Yonsei-ro, Seodaemun-Gu, Seoul 03722, Korea

Table of Contents.....S1

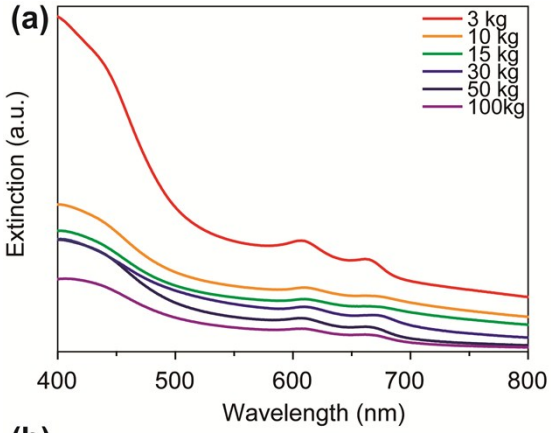

(c)

Centrifugation speed (kg)	3	10	15	30	50	100
Average ζ (mV)	-40.97	-41.2	-39.1	-41.3	-34.73	-30.73

Figure S1. (a) UV-vis-NIR extinction spectra of LA-MoS_2 prepared by different centrifugal forces. (b) The corresponding zeta (ζ) potential distributions. (c) Average ζ of LA-MoS_2 samples.

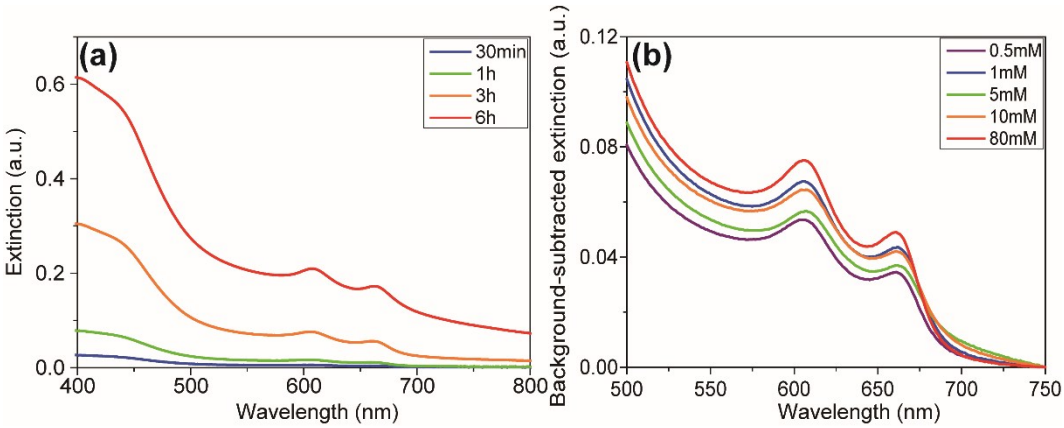

Figure S2. (a) UV-vis-NIR extinction spectra of 5 mM LA-MoS_2 prepared by different sonication time. (b) The corresponding zeta (ζ) potential distributions. (c) Average ζ of LA-MoS_2 samples.

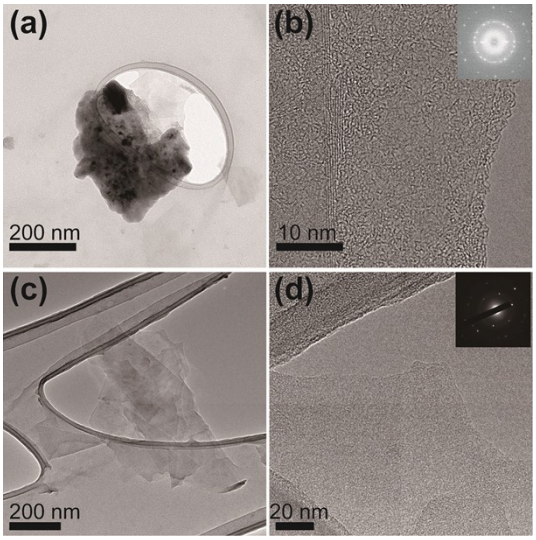

Figure S3. Additional TEM images (a-d).

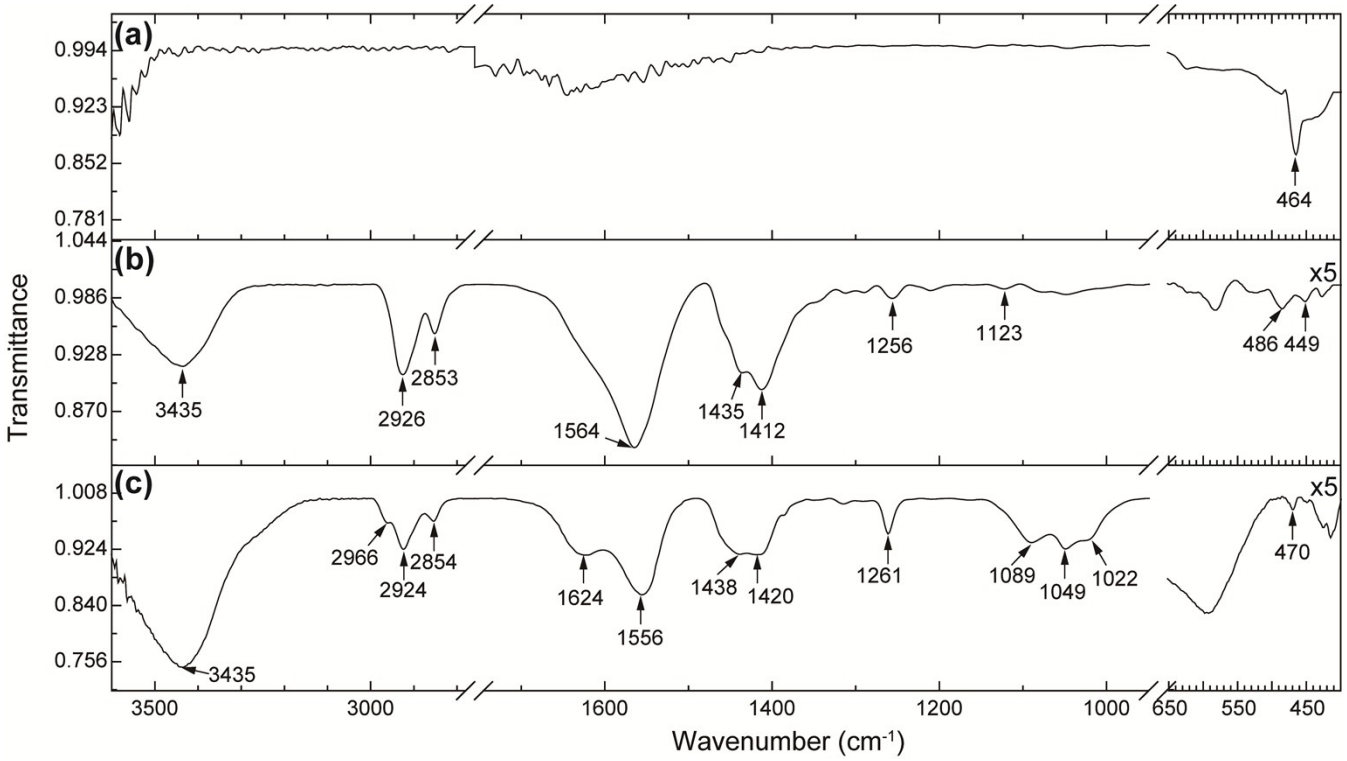

Figure S4. FT-IR spectra of (a) as-MoS_2, (b) LA salt, and (c) LA-MoS_2 conjugate.

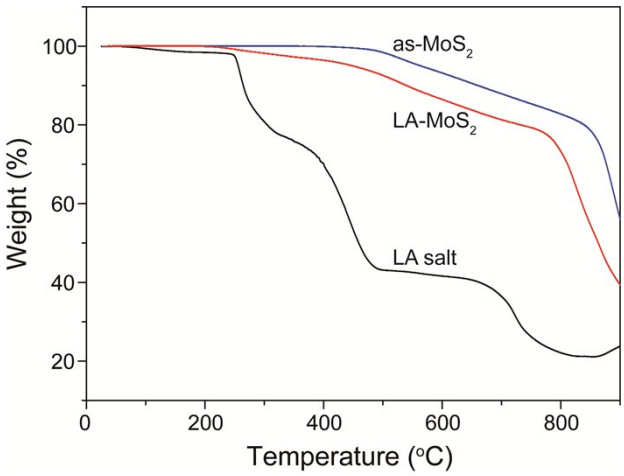

Figure S5. TGA traces of LA salt (black), as-MoS_2 (blue), and LA-MoS_2 conjugate (red).

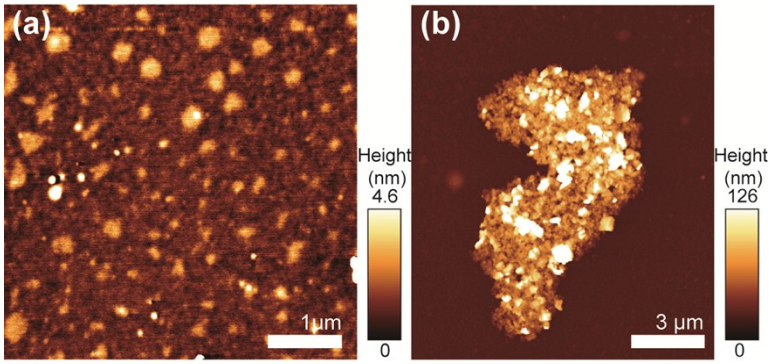

Figure S6. Additional AFM height images of (a) individual LA-MoS_2 conjugate and (b) their aggregates.